Available online at www.sciencedirect.com
ScienceDirect
Earth and Planetary Science Letters 250 (2006) 164–181
EPSL
www.elsevier.com/locate/epsl

Magma degassing and crystallization processes during eruptions of high-risk Neapolitan-volcanoes: Evidence of common equilibrium rising processes in alkaline magmas

G. Mastrolorenzo, L. Pappalardo *

Istituto Nazionale di Geofisica e Vulcanologia, sezione di Napoli Osservatorio Vesuviano Via Diocleziano, 328-80124 Napoli, Italy

Received 2 December 2005; received in revised form 18 July 2006; accepted 18 July 2006
Available online 7 September 2006
Editor: M.L. Delaney

Abstract

Compositional, textural and experimental data on products from explosive and effusive eruptions of Neapolitan volcanoes (Campi Flegrei and Somma-Vesuvio) allow us to constrain degassing and fragmentation conditions during eruptions of alkaline magmas. Significant differences in compositional and textural features have been recognized between lavas, scoria and pumice resulting respectively from effusive, moderately and extremely explosive eruptions. Pumice samples have highly-vesicular glassy matrix, low microlite number density and moderate to high water content. Crystal Size Distributions (CSD) are steep with high intercept values; the narrow microlite size range indicates single nucleation event. Scoria products are characterized by moderate vesicularity and water content. They have high number density of microlites which are bimodal in size. CSD show distinct inflections that are explained as two crystal populations growing in distinct time. Lava samples generally have low vesicularities, moderate to high microcrystalline groundmass and low glass water content. The comparison between textural and compositional features of natural rocks with samples obtained by decompression experiments allows us to conclude that degassing processes during magma ascent occurs in near-equilibrium conditions even at high decompression rate. Moderate to long magma rise times, calculated in the order of a few days, produce open-degassing responsible for moderately explosive to effusive activity. Short magma rise times, calculated in the order of a few hours, result in closed-system degassing that allow explosive fragmentation when the volume of growing bubble reaches a fixed threshold. Vesicularity and water content measured on matrix glass of pumice indicate that this process occurs at pressure of 10–30 MPa. In these conditions, degassing, fragmentation and in turn the eruptive style is strongly influenced by initial conditions in the magma chamber (volatile content, temperature, pressure) instead of decompression rate, in contrast with that observed for rhyolitic melts. These differences have important consequences in terms of volcanic hazards and risk. The low-viscosity alkaline magma is able to maintain efficient degassing even during the final stage of magma ascent, favoring, in the case of closed-system, fragmentation and explosive activity.

Keywords: Campi Flegrei and Somma-Vesuvio; explosive eruptions; vesiculation; crystallization; degassing

1. Introduction

Degassing and crystallization processes related to magma rise in volcanic conduit are crucial issues as they control the style and intensity of volcanic eruptions. Experimental results on bubble growth mostly on

* Corresponding author. Tel.: +39 081 6108444; fax: +39 081 6108351.
E-mail addresses: mastro@ov.ingv.it (G. Mastrolorenzo), lucy@ov.ingv.it (L. Pappalardo).

0012-821X/$ - see front matter © 2006 Elsevier B.V. All rights reserved.
doi:10.1016/j.epsl.2006.07.040

rhyolitic and dacitic volcanic rocks [e.g. 1–8], have indicated that melt viscosity and decompression rate are important factors since they control the transition from equilibrium to non-equilibrium degassing. Equilibrium bubble growth occurs readily in low viscosity melts regardless of decompression rate, whereas bubble–melt equilibrium is not maintained in highly viscous melts at rapid ascent rate. This difference in degassing behavior is thought to hold important implications for the tendencies of highly silicic magmas to generate explosive eruptions, while mafic magmas more often produce moderately explosive or effusive eruptions. On the contrary, other authors [9] carried out experiments on phonolitic magmas which can erupt either explosively or effusively, and demonstrated that alkaline, intermediate-low viscosity melts degas in equilibrium also at rapid ascent rates, up to 20 m/s which are typical of highly explosive eruptions, thus indicating that no simple relationship exists between degassing history and eruption styles.

Recent numerical models [10,11] help to define the influence of different parameters (e.g. vesicularity, crystal content, temperature, water content, conduit geometry) on decompression dynamics during extrusive and explosive eruption regimes. In particular Melnik et al. [11] show that there are at least two regimes for fixed parameters in rhyolitic magma chambers, at equilibrium conditions. The high mass flow rate regime in which magma erupts explosively, and the low discharge rate regime in which fragmentation does not occur and magma erupts effusively.

The high risk alkaline volcanoes of the Campi Flegrei caldera and the Somma Vesuvio, provide a good case study to shed light on this topic as they have typically produced a wide variety of eruptive styles (spanning from plinian to effusive eruptions). Recent textural studies [e.g. 12,13] on Campi Flegrei and Somma-Vesuvius volcanic products have contributed to a better understanding of the mechanism and timing of magma decompression during rise in the volcanic conduit. However for these alkaline magmas, studies relating experimental results with textural and composition of natural rocks are not available.

In this paper we present the results of compositional (matrix glass) and textural (bubble and microlite number density and distribution) studies on a series of samples

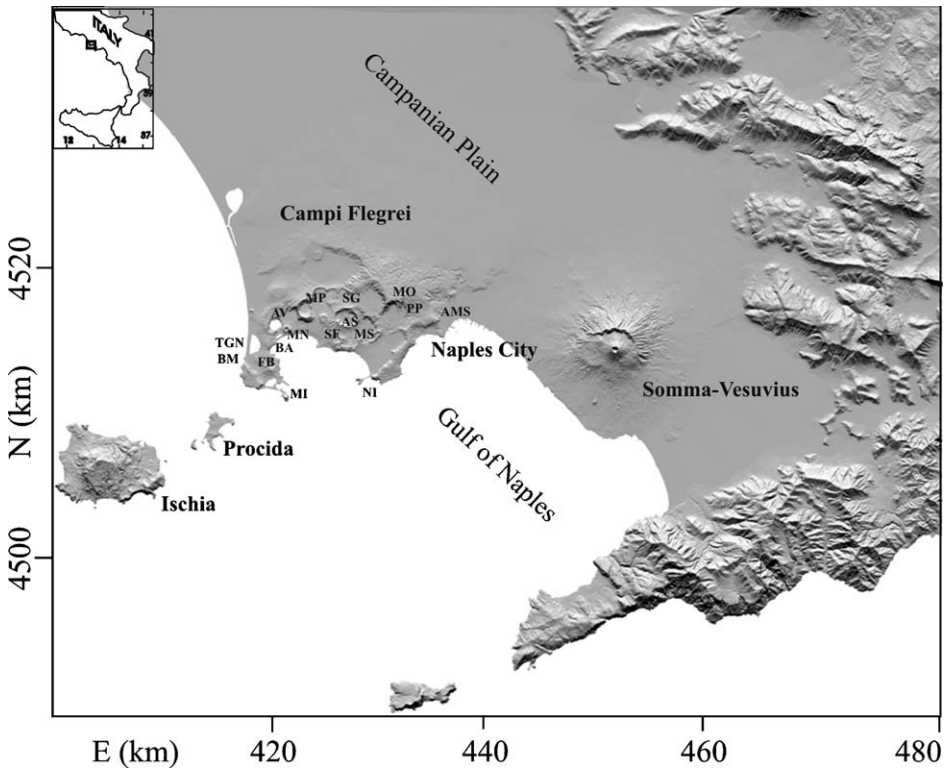

Fig. 1. Location map showing Somma-Vesuvius and Campi Flegrei . AS = Astroni tuff ring; AV = Averno tuff ring; BA = Baia tuff ring; BM = Breccia Museo pyroclastic flow formation; FB = Fondi di Baia cinder cone; MI = Miseno tuff ring; MN = Monte Nuovo cinder cone; MP = Montagna spaccata strombolian formation; MS = Monte Spina small scale pyroclastic flow formation; AMS = Agnano Monte Spina plinian deposit; NI = Nisida tuff cone; SF = Solfatara tuff ring; SG = Senga spatter cone; MO = Minopoli violent strombolian formation; PP = Pomici Principali Plinian formation; TGN = Neapolitan Yellow Tuff.

Table 1
Studied volcanic formations from Campi Flegrei and Somma-Vesuvius volcanoes

Campi Flegrei				Somma Vesuvio			
Volcanic formation	VEI	Age (ka)	Composition	Volcanic formation	VEI	Age (ka)	Composition
Campanian Ignimbrite	7	39	Trachyte/phonolite	Dicco Somma	0	>22.5	Tephrite
Museum Breccia	5	39	Trachyte/phonolite	Sarno plinian eruption	5	22.5	Latite/trachyte
Neapolitan Yellow Tuff	6	14	Latite–trachyte	Ottaviano plinian erupt.	5	7.9	Phonolite
Minopoli	3	11	Trachybasalt	Avellino plinian eruption	5	3.5	Tephrifonolite/phonolite
Pomici Principali	4	10.3	Latite/trachyte	Proto-historic B sub-plin erup.	4	3	Tephrifonolite/phonolite
Montagna Spaccata	3	9.7	Trachyte	79 AD Pompei plinian eruption	5	1.9	Tephrifonolite/phonolite
Baia	3	8.5	Trachyte	472 AD Pollena plinian eruption	4	1.5	Phonotephrite/tephrifonolite
Fondi di Baia	2	8.5	Trachyte	Medioevale stromb eruption	3	0.7	Phonotephrite/tephrifonolite
Agnano Monte Spina	4	4.1	Trachyte	1631 AD sub-plinian eruption	4	0.4	Phonotephrite/tephrifonolite
Monte Olibano	0	4	Latite	1906 AD sub-plinian eruption	3	0.1	Tephrite/phono-tephrite
Solfatara	3	4	Trachyte	1895–99 AD Colle Umberto dome	0	0.1	Tephrite
Averno	3	3.7	Trachyte	1929 AD lava	0	0.07	Tephrite
Astroni	4	3.7	Trachyte	1944 AD strombolian eruption	3	0.06	Tephrite/phono-tephrite
Senga	2	3.7	Latite				
1538 AD Monte Nuovo	2	0.5	Trachyte/phonolite				

VEI = Volcanic Explosivity Index.

spanning the whole Campi Flegrei volcanic field and Somma-Vesuvio strato-volcano history. Our research is carried out in order to investigate the relationship between degassing and crystallization regime with eruptive style, consistent with the results of decompression experiments just available in the literature and of new experiments designed and conducted on the natural samples for this study.

2. Volcanological background

The Campanian Plain, in southern Italy, is one of the Pleistocene–Holocene Italian coastal plains bordering the Tyrrhenian Sea and limited by the Apennine chain. The nearly rectangular flat plain (average 30 m a.s.l), elongated in NW–SE direction, for about 100 km, occupies a wide, graben-like structural depression resulting from a main regional extension produced by the great collision between African and Tyrrhenian plates in the Mediterranean area. The middle-southern part of the Plain is featured by two principal orographic elements: Campi Felgrei volcanic field west of Naples and Somma-Vesuvio strato-volcano, east of Naples (Fig. 1). The onset of volcanic alkaline activity in the Campanian Plain is dated at about 300 ka [14,15], the last eruption occurred at 0.468 ka (1538 A.D. Monte Nuovo) at Campi Flegrei and at 0.062 ka (1944 A.D.) at Somma-Vesuvio.

The Campi Flegrei (CF) is a volcanic field dominated by a quaternary 12-km wide caldera depression formed during two high magnitude eruptions: the 39 ka-BP Campanian Ignimbrite [14] and 14 ka-BP Neapolitan Yellow Tuff [16]. After these two main events, all 60 eruptions occurred in the last 14 ka from scattered vents located within the caldera. A few very large-scale surge and flow deposits occurred during the more prevalent, large explosive eruptions while the tens of intermediate and small-scale deposits occurred as subordinate episodes of more complex eruptive sequences. Effusive activity, with associated lava flows and domes, contributes only a few percent to the total volume of the volcanic products.

Somma-Vesuvius (SV) is a composite strato-volcano consisting of the old edifice of Monte Somma, featured by a summit caldera structure occupied in its center by the younger Vesuvius cone. Volcanic phenomena range from effusive flows to explosive plinian eruptions preceded by long periods of quiescence. During the 20 ka history of Somma-Vesuvius volcano, eight Plinian eruptions occurred, all characterized by high stratospheric convective plumes, phreatomagmatic episodes, pyroclastic flows and lahars. Furthermore, a number of sub-Plinian and smaller scale eruptions generated pumice and ash flows, block and ash flows, rockslide avalanches and lahars. The last 300 years of volcanic activity have been characterized by tens of moderately explosive and effusive eruptions.

The products of both volcanoes belong to the potassic series of Central-Southern Italy Province and range in composition from trachybasalt to trachyphonolite. At Somma-Vesuvius mildly to highly undersaturated rocks, ranging in composition from alkalibasalt to phonolite, also occur.

Geochemical data [e.g. 17–20] indicate the existence of two different reservoirs located at different depths

Table 2
Electron microprobe analyses of matrix glass for Campi Flegrei and Somma-Vesuvius rocks

Samples	CI	CI	NYT	NYT	MIN	PP4L	Ba	Fba	MPP	AMS	AMS	Mol	AV	MN
Formation	Campanian Ignimbrite	Campanian Ignimbrite	Neapolitan Yellow Tuff	Neapolitan Yellow Tuff	Minopoli	Pomici Principali	Baia	Fondi Baia	Montagna Spaccata	Agnano Monte Spina	Agnano Monte Spina	Mt Olibano	Averno	Monte Nuovo
Composition	Trachyte	Trachyte	Latite	Trachyte	Trachybasalt	Latite	Trachyte	Trachyte	Trachyte	Trachyte	Trachyte	Latite	Trachyte	Trachyte
No. anal. spots	(100)	(100)	(80)	(80)	(25)	(25)	(25)	(25)	(25)	(180)	(220)	(25)	(25)	(25)
SiO_2	61.11	64.20	56.92	63.13	52.59	58.17	62.39	62.09	61.13	60.76	61.67	55.98	62.75	61.19
TiO_2	0.41	0.40	0.57	0.33	0.96	0.52	0.39	0.39	0.48	0.53	0.48	0.64	0.40	0.39
Al_2O_3	18.62	19.29	18.32	17.93	18.00	19.45	18.55	18.30	18.63	18.61	18.74	17.82	18.26	20.37
FeO	3.52	1.25	5.59	2.87	7.37	4.42	3.66	3.60	3.48	3.70	3.50	5.88	2.99	2.75
MnO	0.11	0.10	0.11	0.15	0.15	0.15	0.20	0.20	0.17	0.01	0.10	0.15	0.26	0.22
MgO	0.82	0.19	1.71	0.44	4.06	1.13	0.26	0.26	0.59	0.82	0.68	3.35	0.26	0.22
CaO	2.56	1.38	4.94	2.21	10.01	3.76	2.06	2.11	2.46	2.80	2.31	7.02	1.79	1.82
Na_2O	2.96	5.97	3.42	4.28	2.56	3.51	5.41	5.88	4.74	4.02	6.36	3.00	6.60	5.72
K_2O	9.74	7.16	8.08	8.61	3.78	8.72	7.02	7.11	8.23	8.74	5.98	5.72	6.69	7.29
P_2O_5	0.15	0.05	0.35	0.05	0.52	0.18	0.05	0.07	0.11	0.00	0.17	0.42	0.01	0.04
F	0.10	0.10	–	–	0.17	0.22	0.20	0.18	0.19	0.06	0.37	0.20	0.45	0.57
Cl	0.35	0.36	–	–	0.20	0.58	0.50	0.72	0.70	0.59	0.45	0.50	0.86	0.40
S	0.05	0.05	–	–	–	0.12	0.12	0.07	0.08	–	–	0.12	0.05	–
Total	98.90	98.70	97.90	98.90	99.00	94.02	95.22	96.39	96.07	97.70	98.70	97.51	97.03	99.00
Orthoclase	57.58	42.34	47.75	50.90	22.32	51.54	41.46	42.00	48.62	51.66	35.37	33.82	39.52	43.06
Albite	24.78	48.07	16.49	36.01	20.78	18.58	42.70	40.02	31.39	26.82	45.22	24.23	43.78	37.58
Anorthite	8.74	4.66	10.79	4.28	26.49	11.55	5.58	2.53	5.27	6.90	4.89	18.24	0.42	8.39
Nepheline	0.16	1.34	6.73	0.12	0.46	6.03	1.69	5.29	4.70	3.92	4.67	0.65	6.55	5.86
Diopside (Di)	2.57	1.60	9.74	5.47	16.46	5.06	3.79	6.57	5.36	5.99	4.67	11.55	7.32	0.30
Olivine (Ol)	5.07	1.12	6.62	2.48	10.47	5.85	3.93	2.71	3.50	3.71	3.86	9.34	1.62	3.97
Ilmenite (Il)	0.77	0.76	1.08	0.62	1.83	0.98	0.74	0.74	0.90	1.01	0.92	1.21	0.75	0.75
Apatite (Ap)	0.34	0.12	0.81	0.13	1.21	0.42	0.12	0.16	0.26		0.40	0.97	0.03	0.10
Leucite (Lc)	–	–	–	–	–	–	–	–	–	–	–	–	–	–
CaDiSilicate	–	–	–	–	–	–	–	–	–	–	–	–	–	–
Solidification index	13.62	8.76	22.44	12.29	42.20	18.41	11.37	11.27	13.01	14.53	12.72	32.48	9.90	10.35
Differ. ind.	82.52	91.74	70.97	87.02	43.56	76.15	85.85	87.30	84.71	82.40	85.26	58.69	89.85	86.49
Color index	8.41	3.48	17.44	8.58	28.76	11.89	8.45	10.01	9.76	10.70	9.46	22.10	9.69	5.02
Agpaitic index	0.83	0.91	0.78	0.91	0.46	0.78	0.89	0.95	0.90	0.86	0.90	0.62	0.99	0.85
Mg#	29.33	21.67	35.28	21.53	49.55	31.30	11.34	11.38	23.25	28.33	25.78	50.43	13.38	12.48
Olivine fo	1.20	0.22	1.91	0.41	4.49	1.48	0.33	0.23	0.65	0.88	0.81	4.02	0.16	0.37
Olivine fa	3.87	0.90	4.71	2.07	5.98	4.37	3.60	2.48	2.86	2.83	3.05	5.32	1.46	3.60
Diopside wo	1.25	0.78	4.78	2.64	8.25	2.47	1.80	3.12	2.59	2.92	2.27	5.79	3.49	0.14
Diopside en	0.33	0.17	1.53	0.51	3.71	0.70	0.18	0.32	0.55	0.78	0.54	2.61	0.42	0.02
Diopside fs	0.98	0.65	3.42	2.33	4.49	1.88	1.80	3.13	2.22	2.28	1.86	3.14	3.42	0.14

(continued on next page)

Table 2 (*continued*)

Samples	sartl	OPL	A2	A3	ProB	79ad	472	472	1631	1906	1944	1944
Formation	Sarno	Ottaviano	Avellino white	Avellino gray	Proto-historicB	Pompei	Pollena	Pollena	1631	1906 scoria	1944 lava	1944 scoria
Composition	Latite	Phonolite	Phonolite	Phonolite	Phtephrite	Phonolite	Tephrite	Phtephrite	Phonolite	Phtephrite	Phtephrite	Phtephrite
No. analyzed spots	(25)	(25)	(25)	(25)	(25)	(25)	(25)	(25)	(25)	(25)	(25)	(25)
SiO_2	52.74	59.28	57.17	55.93	48.20	61.12	46.44	53.74	58.47	47.64	49.06	48.87
TiO_2	0.51	0.09	0.08	0.29	0.77	0.38	1.26	0.55	0.45	1.23	0.88	0.96
Al_2O_3	20.69	21.87	23.72	21.07	19.41	18.43	17.72	20.09	19.68	17.87	18.12	19.47
FeO	5.90	1.76	1.36	3.55	7.82	3.62	8.67	4.97	3.74	9.44	9.78	8.19
MnO	0.11	0.20	0.09	0.10	0.25	0.15	0.21	0.16	0.15	0.23	0.26	0.20
MgO	1.93	0.05	0.02	1.20	2.09	0.76	3.34	1.47	0.97	3.96	2.71	3.16
CaO	10.56	1.80	1.27	5.11	9.57	2.63	13.27	6.33	3.77	9.94	8.83	9.33
Na_2O	2.90	8.61	9.69	6.06	5.49	4.44	4.34	6.03	5.71	3.49	6.41	3.20
K_2O	4.24	6.33	6.58	6.68	5.29	8.39	4.47	6.28	6.93	5.16	2.77	5.58
P_2O_5	0.42	0.01	0.02	0.01	1.13	0.10	0.29	0.38	0.12	1.04	1.17	1.03
F	0.16	0.69	0.92	0.92	0.50	0.10	0.29	0.55	0.39	0.92	0.53	0.26
Cl	0.28	0.59	0.40	0.40	0.78	0.71	0.48	0.55	0.54	0.40	0.81	0.37
S	0.05	0.03	0.01	0.01	0.02	0.08	0.11	0.05	0.07	0.01	0.03	0.06
Total	97.73	95.64	99.99	99.83	97.62	94.94	95.76	97.70	98.28	99.35	99.42	98.73
Orthoclase (Or)	25.06	37.42	38.91	39.50	23.43	49.56	–	37.09	40.93	25.23	16.39	32.98
Albite (Ab)	16.82	31.40	22.73	15.90	–	30.08	–	10.11	26.37	–	15.43	1.24
Anorthite (An)	30.93	2.34	1.79	10.54	12.71	5.56	15.65	9.21	7.59	17.82	12.47	22.28
Nepheline (Ne)	4.17	22.44	32.09	19.18	25.17	4.08	19.89	22.18	11.91	16.01	21.05	14.00
Diopside (Di)	15.90	5.82	3.88	11.63	23.40	5.89	34.76	16.77	8.82	20.82	20.19	14.59
Olivine (Ol)	5.19	0.39	0.40	2.49	5.11	3.89	3.75	2.73	3.24	11.26	10.11	10.71
Ilmenite (Il)	0.98	0.18	0.15	0.55	1.46	0.72	2.39	1.04	0.86	2.33	1.67	1.82
Apatite (Ap)	0.97	0.01	0.05	0.39	2.61	0.22	0.66	0.88	0.29	2.40	2.72	2.39
Leucite (Lc)	–	–	–	–	6.12	–	–	–	–	4.15	–	–
CaDiSilicate (Cs)	–	–	–	–	–	–	2.19	–	–	–	–	–
Solidification index	44.75	9.75	6.70	23.88	33.98	13.77	43.14	26.80	18.72	35.46	31.76	35.48
Differentiation ind.	46.05	91.26	93.73	74.57	54.72	83.72	19.89	69.38	79.21	45.38	52.86	48.23
Color index	22.06	6.38	4.44	14.67	29.97	10.50	40.90	20.54	12.92	34.41	31.97	27.12
Agpaitic index	0.45	0.96	0.97	0.82	0.76	0.89	0.68	0.83	0.86	0.63	0.75	0.58
Mg#	36.83	5.14	2.55	37.54	32.28	27.16	40.68	34.49	31.50	42.75	33.06	40.76
Olivine fo	1.56	0.01	0.01	0.75	1.32	0.83	1.30	0.76	0.82	4.08	2.68	3.65
Olivine fa	3.63	0.38	0.40	1.74	3.79	3.06	2.45	1.96	2.41	7.18	7.43	7.06
Diopside wo	7.82	2.74	1.82	5.72	11.44	2.86	17.22	8.23	4.31	10.33	9.88	7.22
Diopside en	2.59	0.11	0.04	1.91	3.32	0.70	6.46	2.56	1.23	4.03	2.93	2.67
Diopside fs	5.48	2.96	2.02	3.99	8.63	2.33	11.07	5.97	3.28	6.44	7.38	4.69

Major element concentrations are in weight percent.

Table 3
Concentration of H_2O determined by FT-InfraRed analyses in matrix glass for Campi Flegrei and Somma-Vesuvius samples

Campi Flegrei					Somma Vesuvio				
Samples	Unit	Composition	Thickness in micron	H_2O_{tot} wt.% (stand. dev.)	Samples	Unit	Composition	Thickness in micron	H_2O_{tot} wt.% (stand. dev.)
ICt-t	Campanian Ignimbrite	Trachyte	50 (0.5)	1.4 (0.1)	SARtl-p	Sarno	Trachyte	36 (0.6)	1.4 (0.03)
ICg-t	Campanian Ignimbrite	Trachyte	30 (0.8)	1.6 (0.08)	Ot	Ottaviano	Trachyte	40 (0.8)	1.3 (0.05)
BM-os	Breccia Museo	Trachyte	42 (0.8)	0.5 (0.01)	A1f-p	Avellino	Phonolite	30 (0.5)	1.3 (0.1)
Bm-p	Breccia Museo	Trachyte	40 (0.8)	1.5 (0.1)	A2f-p	Avellino	Phonolite	69 (0.8)	1.2 (0.1)
NYT-p	Neapolitan Yellow Tuff	Trachyte	50 (0.8)	1.4 (0.1)	Atl8-p	Avellino	Phonolite	55 (0.7)	1.5 (0.5)
PP4al-p	Pomici Principali	Trachyte	40 (0.5)	1.8 (0.1)	An-pwhite	Avellino	Phonolite	30 (0.5)	1.9 (0.3)
AS-p	Astroni	Trachyte	30 (1.1)	1.8 (0.1)	An-pgray	Avellino	Tephri-phonolite	30 (0.5)	1.3 (0.3)
AV1006-p	Averno	Trachyte	60 (0.5)	1.5 (0.1)	Avellino	Avellino	Tephri-phonolite	60 (0.8)	0.9 (0.1)
BA-p	Baia	Trachyte	60 (0.5)	1.9 (0.3)	pwhite	Pompei	Phonolite	41 (0.7)	1.8 (0.03)
FBf-p	Fondi di Baia	Trachyte	40 (0.5)	2.2 (0.3)	pgray	Pompei	Tephri-phonolite	45 (0.5)	1.9 (0.06)
SF-p	Solfatara	Trachyte	90 (0.8)	1.8 (0.3)	Es2	Pompei	Tephri-phonolite	60 (0.5)	1.3 (0.1)
MPP-p	Montagna Spaccata	Trachyte	90 (0.7)	1.1 (0.4)	Pn	Pollena	Phono-tephrite	70 (0.5)	1.0 (0.1)
MN11-s	Monte Nuovo	Trachyte	80 (0.8)	1.1 (0.2)	472tl-p	Pollena	Tephri-phonolite	56 (0.69	1.5 (0.2)
MN23-s	Monte Nuovo	Trachyte	75 (0.5)	1.4 (0.2)	1300	Medioevale	Tephri-phonolite	50 (0.6)	1.3 (0.1)
MN31-s	Monte Nuovo	Trachyte	60 (0.8)	0.9 (0.02)	1631-p	1631	Tephri-phonolite	55 (0.6)	0.9 (0.08)
MINp-s	Minopoli	Trachybasalt	100 (0.5)	0.8 (0.02)	1906-p	1906	Phono-tephrite	99 (0.5)	0.7 (0.03)
SN-s	Senga	Latite	70 (0.5)	0.9 (0.02)	Cu-lv	C. Umberto	Tephrite	42 (0.6)	0.5 (0.01)
Molib-lv	Monte Olibano	Latite	70 (0.5)	0.8 (0.02)	29-lv	1929	Tephrite	40 (0.6)	0.1 (0.02)
					44-lv	1944	Tephrite	50 (0.5)	0.2 (0.07)
					44-s1	1944	Phono-tephrite	50 (0.5)	0.1 (0.01)
					44-s3	1944	Phono-tephrite	50 (0.6)	0.2 (0.01)
					Dicco	Somma	Tephrite	38 (0.6)	0.3 (0.01)
					Prb2-p	Proto-historic	Tephri-phonolite	38 (0.7)	0.7 (0.01)

p = pumice; lv = lava; s = scoria; t = tuff; os = obsidian; values by bracket = standard deviation.

that were active under CF and SV volcanoes: a deeper mafic reservoir fed by more primitive magmas may exist beneath the whole Campanian volcanic area, and shallower more evolved magma batches, where assimilation and mixing/mingling processes can occur, are each localized below the individual volcanoes.

Poor constrains on the syn-eruptive conditions for Campi Flegrei and Somma Vesuvio volcanoes are available. Numerical modeling indicate that fragmentation starts at depth ranging between 90 and 50 bar with vesicularity around 0.75% [e.g. 21] for the Neapolitan Yellow Tuff trachytic magmas, while at a depth from 650 to 100 m for the Vesuvius 79 AD phonolite [e.g. 22].

Moreover on the basis of textural studies some authors [12,13,23] suggested that magma rise during explosive events, always occurred at conditions of moderate to low gas oversaturation and in a critical state near the transition between viscosity and diffusivity controlled regime. Subsequent upper level processes (such as magma/water interaction and/or conduit features) control the switching from magmatic to hydromagmatic eruptions.

3. Studied eruptions and sampling strategy

Samples for our study were collected from a representative suite of the explosive (including plinian, subplinian, vulcanian, strombolian types) and effusive eruptive sequence from Campi Flegrei and Somma-Vesuvio. Particularly 13 and 15 different deposits, spanning in a wide range of volcanological features (Table 1) have been chosen for CF and SV, respectively.

These deposits belong to three main types on the basis of eruptive style and composition: (1) pumice fall

and flow deposits derived by high Volcanic Explosivity Index VEI (3–5) eruptions fed by differentiated magmas (trachyphonolite–trachyte for CF and phonolite–tephriphonolite for SV); (2) scoria fall and flow deposits derived by moderately explosive VEI (1–2) eruptions fed by magmas having less-evolved compositions (latite–trachybasalt for CF with exception of Monte Nuovo trachytic deposits and phonotephrite–tephrite for SV); (3) lava flows and domes characterized generally by mafic tephritic composition for SV and by a wider range of composition from trachyte to latite for CF.

Since all chosen formations include vertical and lateral changes as a result of variation in eruptive conditions, we collected samples from the prominent depositional units (considered as type facies) that we assume as representative of the steady-state eruptive phase. This strategy has allowed us to simplify the comparison between samples collected from different types of eruptions. A total of 500 specimens were collected from the distinctive selected units. From each specimen, taken from individual, homogeneous bed sets with clear volcanological features, 0.05–2 cm juvenile clast size fraction has been selected. A preliminary inspection under a binocular microscope has revealed that the clasts of each specimen were mostly homogeneous in morphology, color, macroscopic texture and phenocryst content. A set of tens to hundreds of

Table 4
Clast density and textural parameters for Campi Flegrei and Somma-Vesuvius rock samples

Formation	Bulk density (kg/m^3)	Bulk vesicularity %	Porosity %	BND (bubble/m^3)	BSD slope (mm^{-1})	BSD intercept (mm^{-4})	Crystallinity %	CSD slope (mm^{-1})	CSD intercept (mm^{-4})	Crystal growth time (h)
Campanian Ignimbrite	530	0.8	0.6	9.53E+13	−130.87	18.13	<<1	–	–	–
Museum Breccia	870	0.6	0.5	4.20E+13	−85.33	16.81	<<1	–	–	–
Neapolitan Yellow Tuff	600	0.7	0.4	2.05E+14	−119.33	17.13	<1	–	–	–
Minopoli	810	0.7	0.5	9.20E+13	−72.65	17.22	9	−152	19	11
Pomici Principali	695	0.7	0.4	3.94E+14	−55.90	5.74	<<1	–	–	–
Montagna Spaccata	610	0.7	0.6	9.51E+13	−99.90	23.39	<<1	–	–	–
Miseno	600	0.7	0.7	2.54E+13	−106.70	18.28	<<1	–	–	–
Baia fall	600	0.7	0.6	3.52E+13	−96.50	17.51	5	−7.7	10	211
Baia Mofete	600	0.7	0.5	5.41E+14	−105.05	19.38	<<1	–	–	–
Fondi di Baia	600	0.7	0.5	1.83E+13	−58.20	19.47	<<1	–	–	–
M Spina breccia	725	0.7	0.6	1.61E+13	−75.45	16.10	<<1	–	–	–
M Spina flow	388	0.8	0.4	8.13E+13	−70.00	16.51	<<1	–	–	–
MS. Angelo fall	700	0.7	0.6	1.31E+13	−56.70	14.90	<<1	–	–	–
M Olibano	200	0.2	0.2	1.75E+15	−254.00	19.57	30	−25	13	65
Solfatara	600	0.7	0.4	6.41E+13	−122.00	17.39	<<1	–	–	–
Averno	560	0.8	0.5	2.50E+13	−69.05	15.73	<<1	–	–	–
Astroni	780	0.7	0.6	3.86E+13	−95.27	16.75	<<1	–	–	–
Senga	900	0.7	0.6	2.56E+13	−110.17	18.91	–	–	–	–
Monte Nuovo	1300	0.5	0.4	2.32E+13	−100.00	17.37	32	−36.00	15.80	45
Dicco Somma	2400	0.0	<0.05	4.90E+14	−506.00	21.50	40	−66.4	18.9	25
Sarno Eruption	685	0.7	0.5	1.60E+14	−57.60	15.56	<<1	–	–	–
Ottaviano Erupt	570	0.8	0.6	1.04E+13	−79.40	16.03	1	−80.6	14.1	20
Avellino Eruption	780	0.7	0.6	9.39E+13	−90.90	15.84	2	−117	16.3	14
Pompei Eruption	850	0.6	0.5	1.60E+14	−210.00	19.96	2	−387	20	4
Proto-hist Erupt	1100	0.4	0.4	4.68E+12	−52.40	14.87	3	−162	19	10
Pollena Eruption	1340	0.4	0.4	9.47E+13	−83.65	18.97	2	−108	15.1	15
1300 Eruption	1200	0.4	0.4	1.58E+13	−71.30	17.03	–	–	–	–
1631 Eruption	1350	0.4	0.4	2.08E+14	−127.67	17.75	2	−130	17	13
1906 Eruption	1300	0.4	0.3	1.07E+14	−155.00	16.97	1	−79.1	15.2	21
Colle Umberto lava dome	2000	0.2	0.3	6.11E+13	−464.00	20.43	12	−32.8	14.2	50
1929 lava flow	2200	0.1	0.3	5.87E+14	−339.00	20.82	9	−7.9	9.2	208
1944 explosive phase	1370	0.4	0.2	8.03E+14	−301.00	18.93	2	−60.9	15.7	27
1944 lava flow	2000	0.2	0.2	9.97E+13	−223.00	17.09	7	−36.9	13.5	44

Textural measurements are determined by image analyses; microlite growth time are determined from CSD plots assuming, growth rate G = 1E −7 mm/s consistently with the results from Pinatubo eruptions and our decompression experiments.

Table 5
Experimental conditions and analytical results relative on decompression experimental samples

Experimental conditions						Analytical data of experimental samples				
Sample	Pi (bar)	Pf (bar)	Ascent rate (bar/min)	T (°C)	H_2O wt. %	BND	Porosity %	Slope (mm^{-1})	Intercept (mm^{-4})	H_2O wt.% (FTIR)
PP4AL (A)	1800	150	100/5	900	8	3.1E+13	55	−56.6	14.7	1.21
PP4AL (B)	2000	150	100/2.5	900	8	4.8E+13	45	−203	19.2	1.20
PP4AL (C)	2000	2000	Quenching	950	8	2.0E+14	8	−203	19.5	8.59
PP4AL (D)	2000	150	100/60	950	8	3.8E+13	43	−125	17.9	0.59
AV1006p (D)	2000	150	100/60	950	8	7.2E+12	20	−92.5	16.4	–
PP4AL (E)	2000	1000	100/10	950	8	2.8E+14	10	−349.0	19.3	4.47
AV1006p (E)	2000	1000	100/10	950	8	2.9E+14	16	−246.5	19.5	–
Av1006p (F)	1000	150	100/10	950	8	3.5E+13	–	−139	16.2	–
PP4AL (F)	1000	150	100/10	950	8	1.6E+13	50	−97.6	16.3	1.57

homogeneous, unaltered pumice and lava clasts have been selected and analyzed by using different techniques (including polarized light and Scanning Electron Microscopy, electron microprobe (EMPA), Fourier Transform InfraRed (FT-IR) spectroscopy and laboratory experiments), as described in the following sections.

4. Methods

4.1. Electron microprobe analyses on matrix glasses

Electron probe analyses on polished thin sections were performed on matrix glass of the samples at the "Istituto di Geologia Ambientale e Geoingegneria" (CNR), Roma, Italy, using a Cameca SX-50 electron microprobe. Glass analyses were made by using a 10 μm beam at 15 keV and a beam current of 10 nA, at 10-s counting time. Natural glass standards were used. A defocused beam was used to minimize alkali and volatile loss. In each analysis alkalis (Na, K) and volatile (Cl, F, S) were always counted first, so that diffusion does not affect the analyses. Data reduction was carried out by using the ZAF4/FLS software by Link Analytical. Uncertainty of analysis is in the order of 1% for most elements. Major elements and volatile (Cl, F, S) abundance in matrix glass samples are reported in Table 2. For each pumice and lava samples not less than 25 points in the glass matrix have been analyzed.

4.2. Fourier Transform InfraRed analyses on matrix glasses

FTIR-analyses were performed for water determination in glasses at laboratory of "Dipartimento di Scienze Geologiche" of University "Roma Tre", Rome, Italy. Spectra were collected using a Nicolet Magna 760 FTIR spectrometer using both KBr and CaF_2 beamsplitters, MCT-A detector. A 30 μm diameter, doubly polished area was examined under a Nic-Plan analytical microscope to avoid bubble and surface imperfections. Each spectrum was obtained with 4 cm^{-1} resolution and 128 scans, with the background analyzed throughout the session.

Water concentration was determined using the Beer–Lambert law [24], where: $c=(18.02A/\rho\varepsilon_I d)\times 100$, where c is the molar concentration (in wt.%), A is the intensity of the absorbance peak, ρ is the sample density, ε_I is molar absorptivity for the band of interest (i), and d is the sample the thickness. Molar absorption coefficient of 1.10 and 1.25 L mol^{-1} cm^{-1} were used for the 5200 cm^{-1} (molecular H_2O) and 4500 cm^{-1} (OH–) bands, respectively and 88 L mol^{-1} cm^{-1} was assigned to the 3550 cm^{-1} (H_2O_{tot}) band [25]. Density of the glass is calculated using MELTS program [26]. Absorbance peaks were measured after curved baselines were subtracted. Sample thickness was measured multiple times using a vertically mounted Mitutoyo micrometer, accurate to within ±2 μm. To account for the presence of microlites, measured slab thicknesses were adjusted according to: corrected thickness = (d) (1 − volume fraction of microlites).

The analytical error on any infra-red measurement of water content is estimated to be a maximum of 10% as the effect of uncertainty in density and thickness measurements and error introduced during the measurement of absorption. Results are reported in Table 3.

4.3. Granulometric analyses and bulk density measurements

Grain-size analyses of all the selected pyroclastic samples have been carried out in order to focus structural and textural analyses on clast size interval representative of most of the deposits. Grain-size analyses were performed by dry sieving at one Φ interval in the −4 to 4Φ size range.

Clast density measurements have been carried out for all selected samples. In order to take in account density variations with size, clasts within −5 to 0Φ range were used for density measurements. Sets of 30 clasts for each granulometric class between 0 and −5Φ have been weighted and coated by a thin film of paraffin wax and their average densities have been determined using a picnometer. In order to evaluate a standard deviation in clast density in the same samples, the density of single clast in the range −2 to −5 Φ has been determined individually. We consider the volume of the film of paraffin wax negligible being its density about equal to that of water (1000 kg m^3). For the clast size between 0.5 mm and 10 μm which are not easily measurable with a picnometer, density has been inferred by vesicularity analyses discussed in the following section. Average density for each sample has been calculated (Table 4). The measured clast density has been used to calculate bulk vesicularity (Table 4) for all the selected samples using the non-vesicular juvenile clast density of the composition concerned [as 27].

4.4. Textural measurements

Textural analyses were carried out on polished thin sections of epoxy impregnated grains using a standard polarized light microscope for a preliminary rock characterization, and a Leo-Cambridge 440 scanning electron microscope ("Ingegneria dei materiali" — Facoltà di Ingegneria Università Federico II of Napoli, Italy) for quantitative measurements. For each sample, thin sections from an average of 20 clasts ranging in size between +1 and −5Φ, texturally homogeneous and representative, have been studied. For each clast, at least 10 distinctive areas of ca. 3×10^5 to 3×10^7 μm^2 have been imaged using backscattered electron (BSE) microscope and processed in order to calculate crystal and bubble number density and size distribution. Images are processed and analyzed using Adobe Photoshop and NIH Image 1.60 software. The images have been first reduced to binary images and then manipulated to reduce noise and to separate individual crystals and vesicles. Crystal and bubble size distributions were obtained by using CSD Corrections 1.3 program [28,29] that includes corrections for both the intersection probability and the cut section effects.

4.5. Decompression experiments

Constraints on degassing regime and decompression rate are already available in literature for phonolitic melts similar to that erupted at Somma-Vesuvius [9] therefore in order to retrieve constrains for CF trachytic samples a set of new decompression experiments on the selected samples at different conditions has been carried out at La Sapienza University of Roma, laboratory of experimental petrology. All experiments were run in 3 mm diameter Pt capsules using an Externally Heated Pressure Vessel (type TZM).

Powder samples of 5 μm size were obtained by hand crushing pumice clasts from plinian Pomici Principali and Averno tuff ring eruptions of Campi Flegrei. Pumice consists of clear, vesicular, trachytic glass with less than 5–10% vol of phenocrysts of sanidine, and minor clinopyroxene, biotite, magnetite, major composition is reported in Table 2.

In our experiments were carried out at different initial conditions and decompression rate and water content

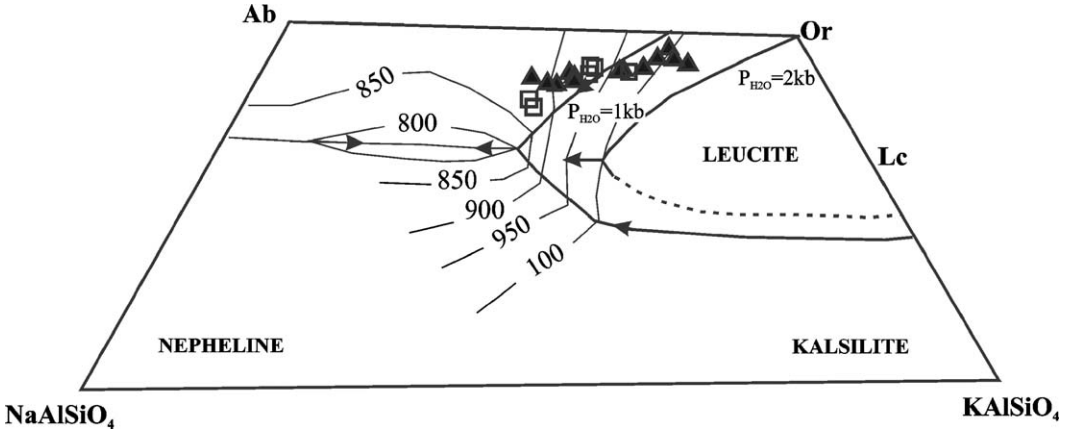

Fig. 2. Matrix glass compositions of Campi Flegrei and Somma-Vesuvius rocks projected onto the Petrogeny Residua System. Symbol: squares = Campi Flegrei samples; triangles = Somma-Vesuvius samples.

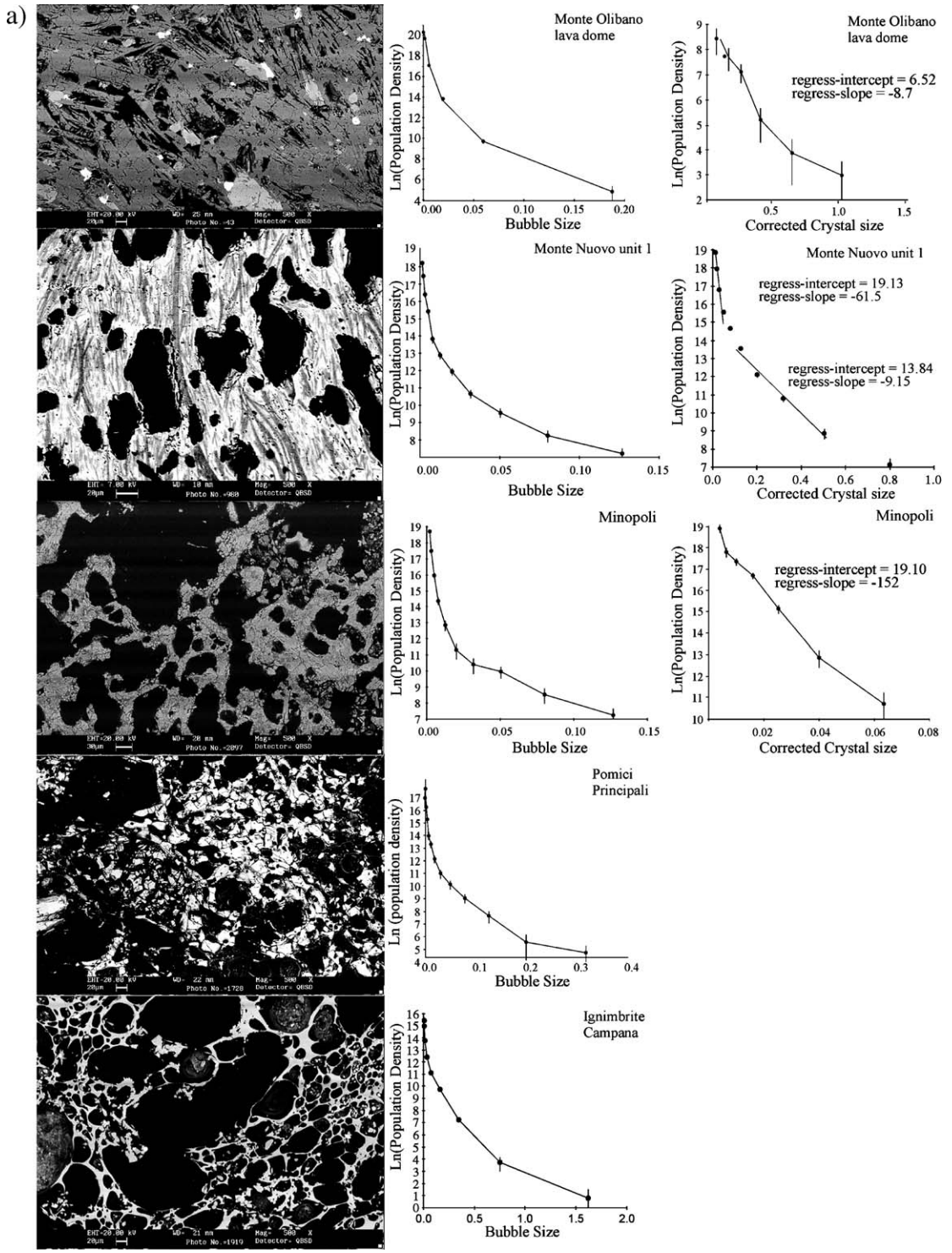

Fig. 3. Backscattered electron microscope (BSE) images of representative Campi Flegrei and Somma-Vesuvius rock types, with the relative CSD and BSD. CSD are not reported for Campanian Ignimbrite and Pomici Principali samples which have microlite-free glass groundmass.

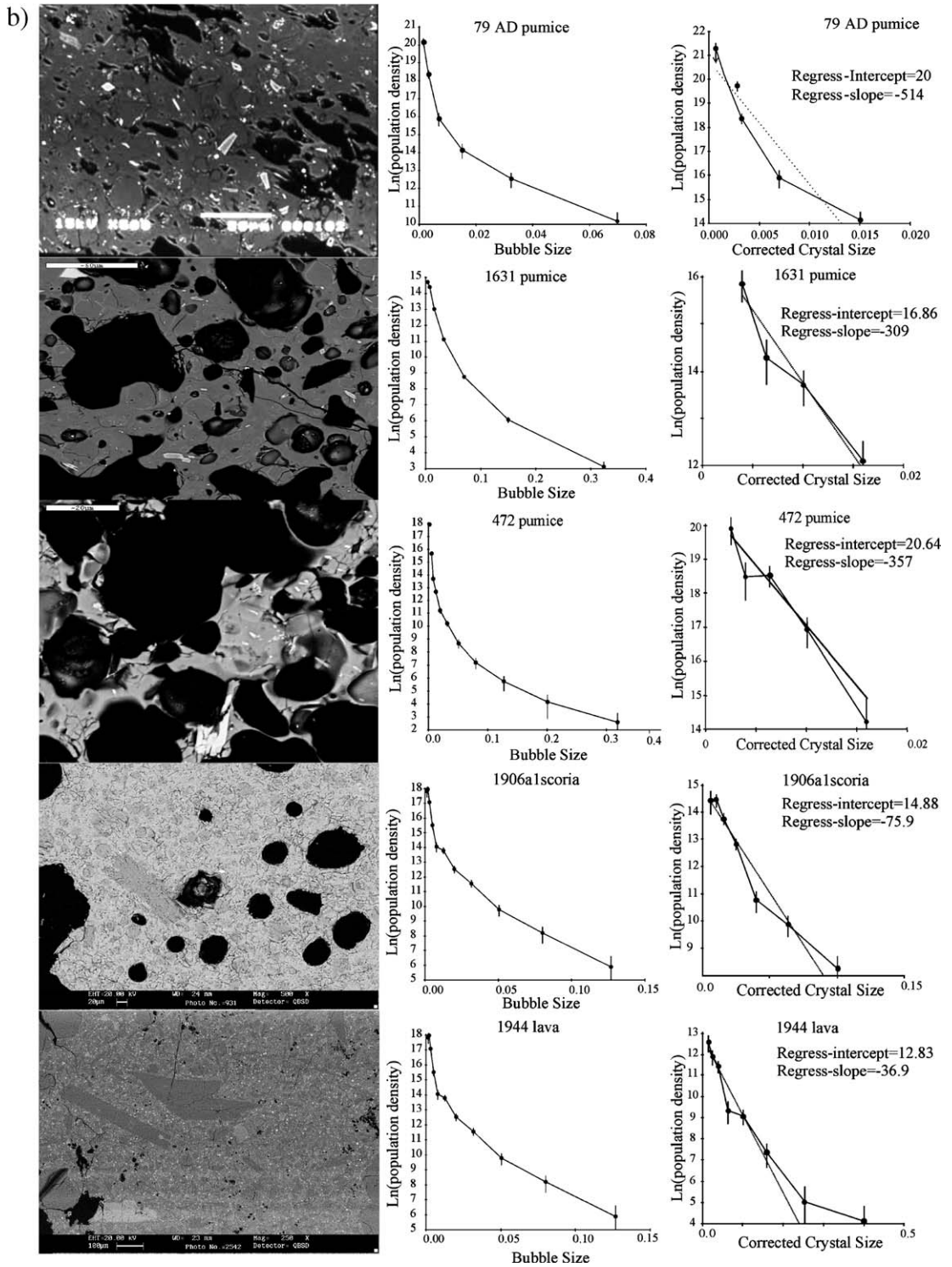

Fig. 3 (*continued*).

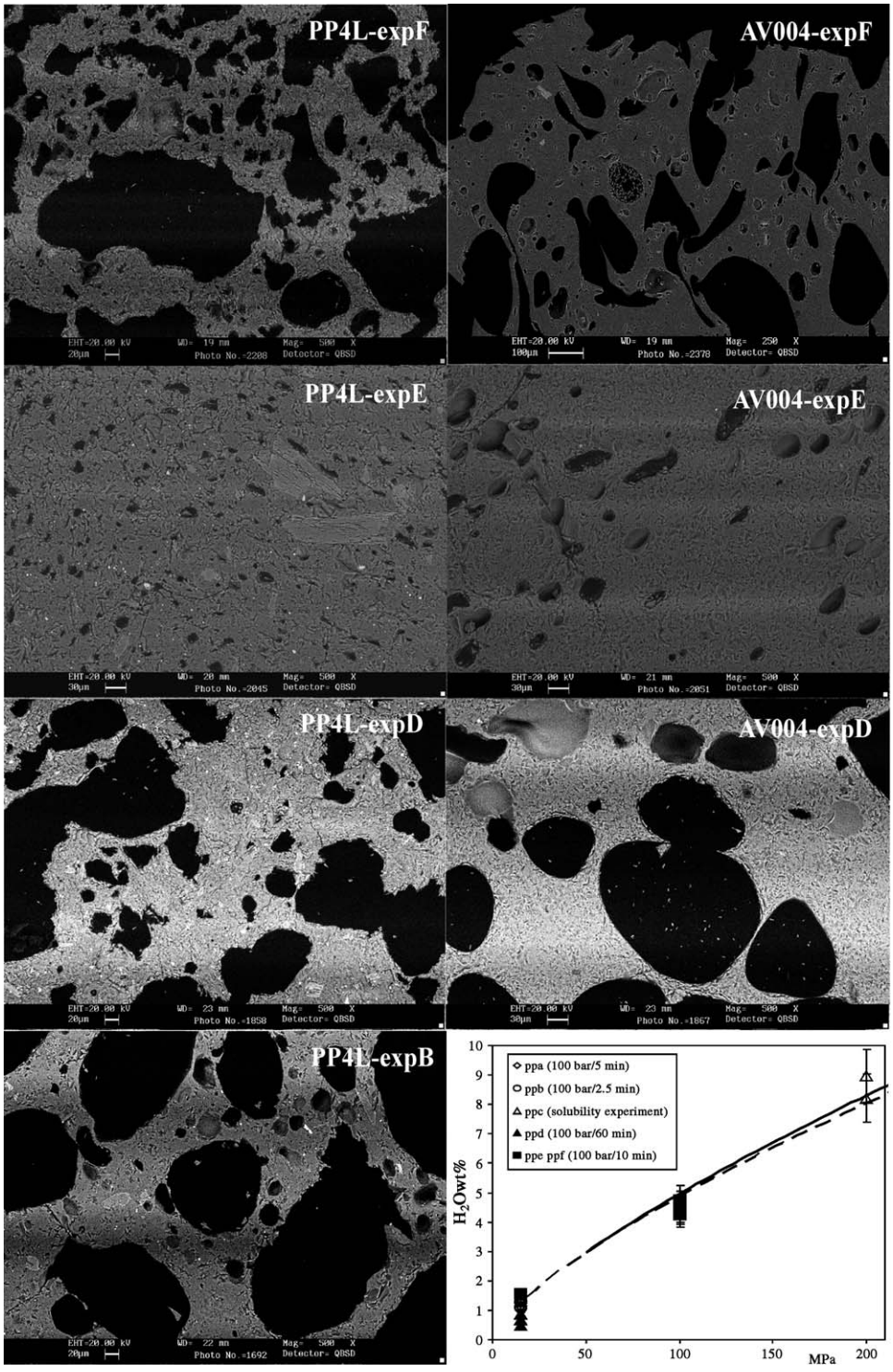

Fig. 4. Backscattered electron microscope images (BSE) of specimens produced in decompression experiments. See Table 5 for experimental conditions and analytical results. In the low left corner: plot of glass water content versus final pressure of our experimental samples. Experimental equilibrium curves (Tenerife phonolite by Carroll and Blank, [25] and Laacher See phonolite [9]) are also shown.

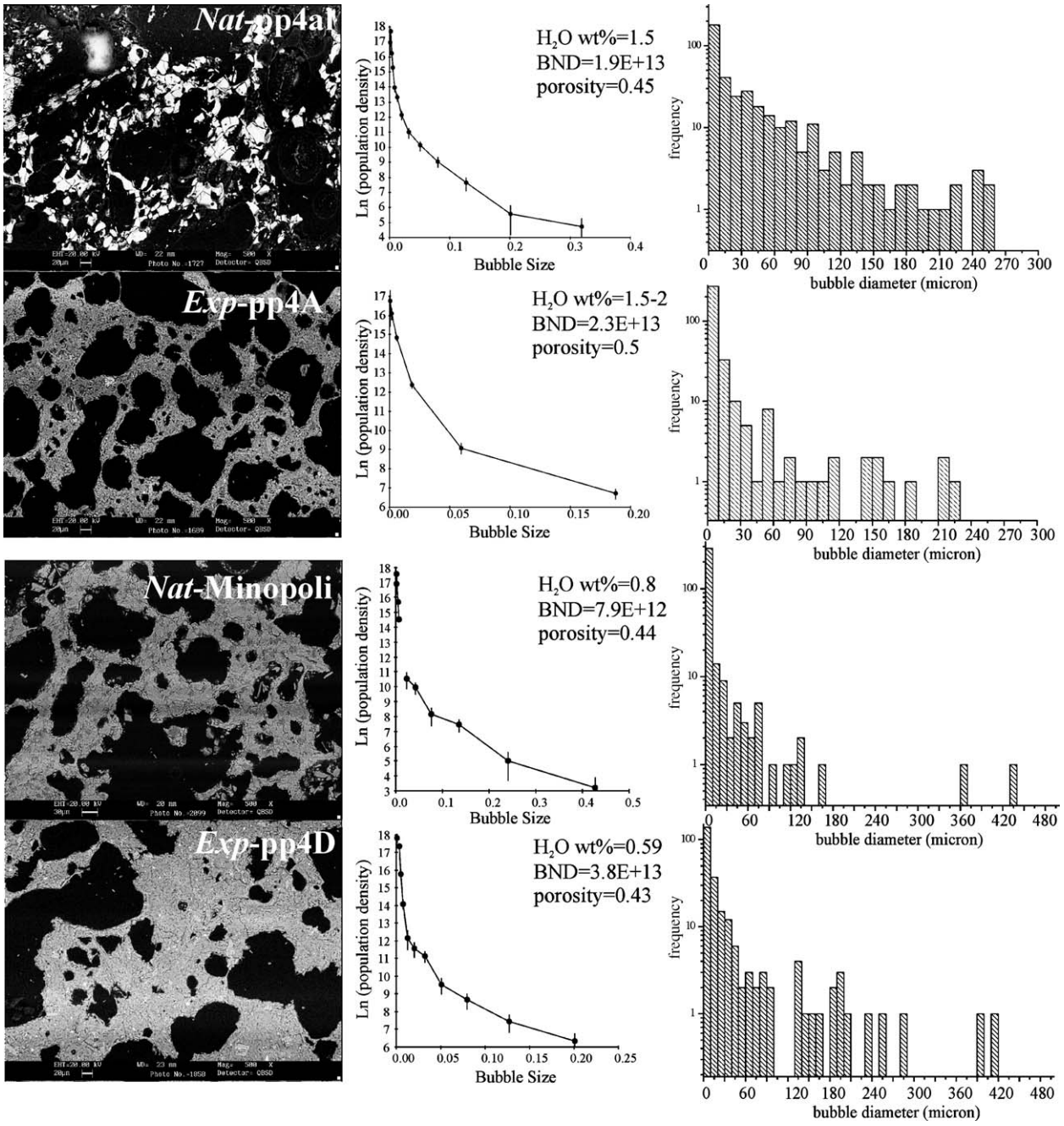

Fig. 5. Textural features and water content of representative experimental and natural samples.

and textural features have been measured for the specimens produced in our decompression experiments (Table 5).

Initial water content, temperature and pressure has been fixed for all experiments at 8 wt.%, 950 °C, and 200 MPa respectively, in order to reproduce the magma chamber conditions inferred from our glass composition and literature data. The decompression rate is 100 bar every 10, 5, 2.5 min, typical of explosive eruptions and in analogy with the rising time calculated by our CSD for CF and SV explosive eruptions. In one experiment the decompression rate is fixed to 100 bar every 60 min to simulate effusive conditions. One experiment (experiment C in Table 5) was conducted by quenching the sample after water saturation without pressure release to determine equilibrium water solubility at 200 MPa.

5. Results

5.1. Major element and volatile (Cl, F, S) concentrations in matrix glasses

Glass in our Campi Flegrei and Somma-Vesuvius pumice has homogeneous trachytic and phonolitic composition, respectively, while scoria and lavas have less evolved composition ranging from latite to trachybasalt for CF and from phono-tephrite to tephrite for SV (TAS diagram, [30]).

Cl and F contents range from 0.5 to 0.6 wt.% and from 0.2 to 0.6 wt.%, respectively for CF trachytic–latitic pumice, and from 0.3 to 0.7 wt.% and from 0.2 to 0.8 for phonolitic–tephritic Somma-Vesuvius samples, while S content generally is lower than 0.1 wt.%.

Evolution of the melt composition is illustrated by projection of glass composition on the Petrogeny Residua System (Fig. 2). When projected onto the Ne–Ks–Si ternary diagram, matrix glass compositions show that melt composition is compatible with PH_2O between 2 and 1 kbar and T between 850 and 950 °C.

5.2. Water concentration in matrix glasses

Water content ranges between about 1 and 2.0 wt.% for SV phonolitic and CF trachytic pumice glass (Table 3). These values are typical also of other most highly explosive evolved eruptions (e.g. dacitic pumice from Pinatubo 1991 eruptions [31] and rhyolitic pumice from Monte Pelee volcano in Martinique [32] and from Tenjo eruption in Japan [33]).

Speciation data following [25] indicate that water contents in the glass groundmass is always magmatic with the only exception of few glass water-rich CF products (not reported in Table 3), which probably were effected by syn-eruptive magma/water interaction and/or syn-depositional alteration processes [e.g. 34].

Glass in obsidian (Breccia Museo trachytic deposit), in CF trachybasalt-latitic and SV tephritic strombolian and effusive products exhibit generally lower water contents (0.1–0.8 wt.%) than products of explosive eruptions.

CO_2 content is always under the detection limit for both CF and SV glass.

5.3. Granulometric analyses and clast density

Results indicate that Md_Φ range for all samples between −2 (4 mm) and 2 (1/4 mm) Φ with σ_Φ ranging between 0.5 and 2.5.

Pumice clasts, from highly explosive eruptions, show the minimum density values from 500 to 800 kg/m^3 and porosity from 40 to 60%; scoria and lava clasts, from moderately explosive and effusive activity, exhibit high density from 1000 to 1500 kg/m^3, and from 2000 to 2500 kg/m^3, respectively (porosity ranging from 10 to 20% and from 40 to 45%, respectively).

5.4. Clast texture

We did not observe systematic differences in vesicle texture between Campi Flegrei and Somma-Vesuvius samples. Major differences are observed between pumice from highly explosive eruptions, and scoria and lavas from moderately explosive and effusive activity (Table 4 and Fig. 3).

Generally pumice samples have low density (0.5–0.7) and are highly vesicular (0.8–0.7); bubbles are rounded and often coalesced, size distributions are normally polymodal, with a prevalent (80%) smaller bubble population, with a peak at 10–20 μm and a subordinate (10–15 vol.%) coarser population (100–200 μm) probably resulting from bubble coalescence, as suggested by frequent wall remnants of former smaller bubbles. The groundmass of pumice from highly explosive Campi Flegrei eruptions are generally microlite-free, and are either microlite free- or microlite bearing (with up to 20 vol.% microlites on a bubble-free basis determined by image analysis) for Somma-Vesuvio rocks.

Scoria and lava samples have generally moderate density (0.8–1.2) and bulk vesicularity (0.6–0.4). Vesicles are smaller and less rounded with respect to pumice. Bubble size populations are general bimodal. The groundmass of scoria and lava samples of both CF and SV are richer in microlites (up to 50 vol.% determined by image analysis), with average crystal sizes ranging from a few microns to 50 μm. Microlite phases generally are acicular feldspars for Campi Flegrei samples, and abundant leucite, minor feldspar, pyroxene, amphibole, and mica for Somma Vesuvio.

5.4.1. Bubble number density and size distribution

Bubble number density (BNd) is obtained by solving the following equation for Nd: Vo=(c1r13+c2r23+…..+cnrn3)4/3πBNd, where Vo is the calculated void fraction, r1 is the radius of the bubble in the class size "1", c1 is the determined volume fraction of the class "1" (Fig. 3) [12].

Bubble number density ranges for most samples from ca. 10^{12} to 10^{14} bubble/m^3 regardless of the eruptive style (Table 4 and Fig. 3). Bubble size distributions for representative samples have been obtained plotting the natural log of the population density versus bubble length, following Klug et al. [35]. In this plot (Fig. 3) the

BSD of all the considered samples shows close values of slope and intercept (Table 4) indicating a possible recurrent bubble nucleation and growth regime.

5.4.2. Microlite number density and distribution

Crystal size distributions have been analyzed according to the crystal size distribution theory by Marsh [36]. The theory allows defining quantitatively the nucleation and growth rate of crystals, respectively on the basis of intercept and sloping values obtained by the size population distribution. As defined in Marsh equation, the slope is the inverse product of the growth rate and residence time, which could be assumed to represent the crystal growth time during ascent through the conduit. Therefore assuming that the growth rate is constant, higher slopes are indicative of fast ascent rate. The nucleation rate is the product of the average growth rate and the number density of crystals having zero size (*y*-intercept value), so that higher intercept values are indicative of higher nucleation rate. The application of the Marsh [36] CSD method has proven successful to investigate magma ascent dynamic during historical and recent explosive and effusive eruptions for which the dynamic and timing of each phase of the eruption are known in detail (e.g. 1991 eruption from Mt. Pinatubo, Philippines [31], 1989–1990 eruptive activity at Reboubt Volcano, Alaska [37], 1538 Monte Nuovo eruption, Campi Flegrei [13]). In CSDs cal culations we use the average growth rate (1.7E−7 mm/s) measured for products emitted during observed explosive eruptions [31] that corresponds to minimum growth rates of microlites observed in decompression experiments [e.g. 1,6–8].

Slope and intercept values of CSDs, computed by plotting the natural log of the population density versus crystal length (CSDs), span over a wide range and are broadly correlated with eruption style (Fig. 3 and Table 4). Steeper slopes (−300) and higher intercept values (18) characterize pumice samples from explosive eruption; intermediate values, slope around −80 and intercept around 15, are generally observed in scoria from strombolian deposits; while gentle slopes (−25) and lower intercept values (12) are characteristic of lava samples.

Results of decompression experiments [e.g. 7,8] demonstrated crystal nucleation induced by decompression occur after a delay of 1–4 h, and that after this lag crystallization can be rapid and extensive and will re-establish equilibrium. A fast depressurization will not permit significant crystallization, whereas, if the depressurization rate is low, crystallization can be significant and maintain equilibrium. On this basis, the poor microlite content in CF and SV pumice erupted from high explosive eruptions is consistent with high ascent rate in the order of hours (steep slopes with higher intercept in CSDs); in contrast their abundance in scoria and lavas from strombolian to effusive events, indicate a relatively low ascent rate in the order of days (shallow slopes with lower intercepts in CSDs).

5.5. Experimental constraints on degassing regime

In the quenched sample phenocrysts present in the starting powder did not dissolve entirely, these residual crystals, less than 1 wt.% of the sample, are easily recognizable by crystal morphology and are deleted digitally from the analysis and have minimal influence on the measured textural parameters. Some authors [2] reported the presence in not decompressed samples of hydration bubble (from 0.5 to 9 vol.%) that are considered original spaces between powder grains, in our samples we observe an irrelevant percentage of very small hydration bubbles, so that we can consider that all bubbles present in the experimental samples grew during decompression.

Water contents and vesicularities measured in our decompressed samples agree with that calculated at equilibrium conditions in a closed-system regime (Table 5 and Fig. 4), thus indicating that at the time scale of the experiments the equilibrium degassing is obtained even at the short rising time. A good correlation has been detected (Fig. 5) between textural and compositional features of decompressed with natural samples. These analogies and the correspondence between the experimental decompression rate with the inferred minimum rising time in real eruptions (in the order of tens of minutes to hours calculated on the basis of microlite distribution) strongly support closed system equilibrium degassing conditions during explosive eruptions of CF and SV.

6. Discussion

Recent numerical models [10,11] have contributed to investigate the influence of different parameters (e.g. vesicularity, crystal content, temperature, water content, conduit geometry) on decompression dynamics during extrusive and explosive eruption regime. The results of our study on effusive and explosive eruptions of Neapolitan volcanoes allow a comparison between the parameters inferred from the models with those found through studies of natural samples and decompression experiments and to define quantitatively their influence on the eruptive mechanism. The fundamental questions we have investigated are: (1) the influence of magma composition and pre-eruptive conditions on eruptive style; (2) the importance of degassing regime (disequilibrium/equilibrium, closed/open system) in controlling bubble growth in

conduit and thus magma rising processes; (3) the mechanism and depth of magma fragmentation.

Major differences characterize the three main groups of analyzed CF and SV rocks: (a) lavas, (b) scoria and (c) pumice resulting respectively from effusive, moderately and extremely explosive eruptions.

Pumice always show high to moderate vesicularity (0.6–0.8) and water content (1–2 wt.%). These clasts have abundant spherical and partially coalesced vesicles in microlite-poor to microlite-free groundmass glass. They are characterized by low number density of prismatic feldspar microlite (CF and SV samples) and/or sparse mafic microlites (SV samples) within a glassy matrix. CSD are steep and have high intercept values, the narrow microlite size range indicates single nucleation event. Scoria products are characterized by moderate vesicularity (0.6–0.4), microlite and water content (<1 wt.%). Vesicles are small and irregular in shape. They have higher number density of microlites which are bimodal in size. CSD show distinct inflections that are interpreted as two crystal populations growing in distinct time. Lava samples are generally mostly featured by low vesicularity (0.4) and glass water content (0.1 wt.%), moderate to high microcrystalline groundmass of plagioclase, cpx and Fe–Ti oxides.

These characteristics reflect different conditions of degassing and crystallizations. According to the recent literature [e.g. 6–11,38] vesicularity, microlite abundance and glass volatile content are the integrated result of magma chemico-physical proprieties (viscosity and volatile content), as well as decompression/degassing regime and rate. In particular, in low decompression rate typical of effusive and poorly explosive eruptions, open system conditions can be achieved thus producing low rock vesicularity and glass volatile content and effective microlite growth by degassing induced-crystallization processes. On the contrary, high ascent rates lead to closed system degassing conditions, and high magma vesicularity, final volatile contents that inhibited microlite nucleation and growth.

The observed vesicularity of CF and SV pumice (70–80%) is consistent with that calculated [39] in the case of a closed-system degassing. Moreover CSD data on our pumice samples are consistent with rapid magma ascent, in the order of tens of minutes to a few hours. By contrast, the nearly dry matrix glasses of dense scoria and lavas are consistent with magma degassing under open system conditions, probably allowed by long ascent time scale in the order of days to weeks as indicated by our CSD data.

Numerical and experimental studies on viscous melts indicate that rapid magma ascent is generally associated with degassing in disequilibrium conditions, which is thought to induce explosive eruptions. Even if our data on natural samples do not allow us to unequivocally constrain degassing conditions, merged results from analytical and experimental studies indicate that both phonolite and trachyte, due to their low viscosity, degas generally at equilibrium conditions over a wide range of decompression rates typical of most explosive eruptions [9,40]. These, in agreement with the results of our decompression experiments, confirm that at water saturation conditions and an initial chamber pressure of 200 MPa, vesiculation occurs in equilibrium even during decompression at rates at least up to 0.1 MPa/s.

Nevertheless, consistently with results from Na-phonolitic explosive rocks from other volcanoes (Laacher See phonolite, [9] and Tenerife phonolite, [25]), our results on K-phonolite and trachyte indicated that water dissolution into melts is probably more controlled by Al and Si than alkalis. This implies that constrains on degassing in alkalic magmas should apply equally well to both high Na and K series.

In the inferred equilibrium degassing conditions, the water content, measured in matrix glass in our products from high explosive eruptions, closely represents the residual dissolved water content in the melt at the fragmentation level. Considering the relationship between pressure and water content obtained experimentally for phonolite [25] and trachyte (Carroll, personal communication) at temperatures of 850–900 °C, the measured water content in glass of our natural samples (1–2 wt.%) corresponds to a fragmentation level of 10–30 MPa (300–1000 m), with the obtained vesicularity in the order of 70–80%, which is very close to the bubble packing state conditions for magma fragmentation [40]. Nevertheless, this conclusion is consistent with quite homogeneous clast vesicularity observed in all studied pyroclastic deposits and allows us to conclude that for CF and SV products, magma fragmentation occurs after bubble expansion when a fixed gas volume threshold is reached (bubble packing state). Other fragmentation mechanisms, particularly brittle failure theory [e.g. 41,42] and gas bubble overpressure criterion [e.g. 43], generally invoked for highly viscous rhyolitic magmas, can be excluded for alkaline SV and CF explosive eruptions. In fact, the last two fragmentation mechanisms are not dependent on the extent of vesiculation but are consequence of the cumulative strain of bubble growth. They imply water over-saturation for resulting pyroclastic products [e.g. 2], and typical tube texture of pumice [42], features not observed in studied CF and SV samples. This conclusion indicates that degassing, fragmentation and thus eruptive style for the studied products strongly depends on pre-eruptive magma composition, volatile content and storage depth.

7. Conclusion

The results of our study provide evidence of equilibrium degassing with relatively short magma ascent time both in explosive and effusive eruptions of Campi Flegrei and Somma-Vesuvio. These features could have important consequence in terms of volcanic hazard and risk. The low-viscous alkaline magmas are able to maintain efficient degassing even during the final stage of magma ascent, driving magma fragmentation and explosive eruptions. The investigation of timing of the eruptive processes is fundamental to understand the behavior of geochemical and geophysical precursors. In fact, recent textural and compositional studies on historical (1538 Monte Nuovo at Campi Flegrei, [13]) and recent eruptions (e.g. 1991 Mt. Pinatubo at Philippines, [31]; 1995 Soufriere Hill at Montserrat, [7,8,44]; 1980 Mount St. Helens at WA, [45]) have confirmed that degassing and crystallization mechanisms in conduit could be strongly related to the appearance and behavior of eruption precursors. Months to days before the eruptions magma chamber fracturing and magma degassing processes could be the source of ground deformation, superheated steam, and seismicity. Our inferences on the rise processes timing retrieved from CSD data for CF and SV rocks, allow us to make some speculation about a possible reliable forecast of magmatic activity for these volcanoes in the order of tens of hours before eruptions.

Acknowledgement

The authors wish to thank Marcello Serracino (Centro Studio per il Quaternario e l'Evoluzione Ambientale, Roma, Italy) for kind assistance during electron microprobe analyses and dott. B. Di Vita ("Ingegneria dei materiali" — Facoltà di Ingegneria University of Naples "Federico II", Italy) for his contribution during SEM analyses. We are thankful to dott. G. Della Ventura (University "Roma Tre", Rome, Italy) for his help during FT-IR analyses. Prof. Raffaello Trigila (University of Rome "La Sapienza", Italy) is gratefully acknowledged to consent decompression experiments. The comments and suggestions of two anonymous referees are greatly appreciated.

References

[1] C.H. Geschwind, M.J. Rutherford, Crystallization of microlites during magma ascent: the fluid mechanism of 1980–1986 eruption at Mount St Helens, Bull. Volcanol. 57 (1995) 356–370.
[2] J. Gardner, M. Hilton, M.R. Carroll, Experimental constraints on degassing of magma: isothermal bubble growth during continuous decompression from high pressure, Earth Planet. Sci. Lett. 168 (1999) 201–218.
[3] M.T. Mangan, L.G. Mastin, T. Sisson, Gas evolution in eruptive conduits: combining insights from high temperature and pressure decompression experiments with steady-state flow modeling, J. Volcanol Geotherm. Res. 129 (2004) 23–36.
[4] M.T. Mangan, T. Sisson, Delayed, disequilibrium degassing in rhyolite magma: decompression experiments and implications for explosive volcanism, Earth Planet. Sci. Lett. 183 (2000) 441–455.
[5] C.C. Mourtada-Bonnefoi, D. Laporte, Kinetics of bubble nucleation in a rhyolitic melt: an experimental study of the effect of ascent rate, Earth Planet. Sci. Lett. 218 (2004) 521–537.
[6] J.E. Hammer, M.J. Rutherford, Magma storage prior to the 1912 eruption at Novarupta, Alaska, Contrib. Mineral. Petrol. 144 (2002) 144–162.
[7] S. Couch, C.L. Harford, R.S.J. Sparks, M.R. Carroll, Experimental constraints on the conditions of formation of highly calcic plagioclase microlites at the Soufriere Hills Volcano, Montserrat, J. Petrol. 44 (2003) 1455–1475.
[8] S. Couch, R.S.J. Sparks, M.R. Carroll, The kinetics of degassing-induced crystallization at Soufriere Hills Volcano, Montserrat, J. Petrol. 44 (2003) 1477–1502.
[9] J. Larsen, J. Gardner, Experimental study of water degassing from phonolite melts: implications for volatile oversaturation during magmatic ascent, J. Volcanol. Geotherm. Res. 134 (2004) 109–124.
[10] A. Proussevitch, Sahagian, Bubbledrive-1: a numerical model of volcanic eruption mechanisms driven by disequilibrium magma degassing, J. Volcanol. Geotherm. Res. 143 (2005) 89–111.
[11] O. Melnik, A.A. Barmin, R.S.J. Sparks, Dynamics of magma flow inside volcanic conduits with bubble overpressure buildup and gas loss through permeable magma, J. Volcanol. Geotherm. Res. 143 (2005) 53–68.
[12] G. Mastrolorenzo, L. Brachi, A. Canzanella, Vesicularity of various types of pyroclastic deposits of Campi Flegrei volcanic field: evidence of analogies in magma rise and vesiculation mechanisms, J. Volcanol. Geotherm. Res. 109 (2001) 41–53.
[13] M. Piochi, G. Mastrolorenzo, L. Pappalardo, Magma ascent and eruptive processes from textural and compositional features of Monte Nuovo pyroclastic products, Bull. Volcanol 67 (2005) 663–678.
[14] B. De Vivo, G. Rolandi, P.B. Gans, A. Calvert, W.A. Bohrson, F.J. Spera, H.E. Belkin, New constraints on the pyroclastic eruptive history of the Campanian volcanic Plain (Italy), Mineral. Petrol. 73 (2001) 47–65.
[15] D. Brocchini, C. Principe, D. Castradori, M.A. Laurenzi, L. Gorla, Quaternary evolution of the southern sector of the Campanian Plain and early Somma-Vesuvius activity: insights from the Trecase 1 well, Mineral. Petrol. 73 (2001) 67–91.
[16] A.L. Deino, G. Orsi, S. de Vita, M. Piochi, The age of the Neapolitan Yellow Tuff caldera-forming eruption (Campi Flegrei caldera — Italy) assessed by $^{40}Ar/^{39}Ar$ dating method, J. Volcanol. Geotherm. Res. 133 (2004) 157–170.
[17] L. Pappalardo, M. Piochi, M. D'Antonio, L. Civetta, R. Petrini, Evidence for multi-stage magmatic evolution during the past 60 ka at Campi Flegrei (Italy) deduced from Sr, Nd and Pb isotope data, J. Petrol. 43 (2002) 1415–1434.
[18] G. De Astis, L. Pappalardo, M. Piochi, Procida Volcanic History: new insights into the evolution of the Phlegraean Volcanic District (Campania region, Italy), Bull. Volcanol. 66 (2004) 622–641.
[19] L. Pappalardo, M. Piochi, G. Mastrolorenzo, The 3800 yr BP–1944 AD magma plumbing system of Somma-Vesuvius: constraints on its behavior and present state through a review of isotope data, Ann. Geophys. 47 (2004) 1471–1483.

[20] G. De Natale, C. Troise, F. Pingue, G. Mastrolorenzo, L. Pappalardo, The Somma-Vesuvius Volcano (Southern Italy): structure, dynamics and hazard evaluation, Earth Sci. Rev. 74 (2006) 73–111.
[21] K. Wohletz, G. Orsi, S. de Vita, Eruptive mechanism of the Neapolitan Yellow Tuff interpreted from stratigraphic, chemical and granulometric data, J. Volcanol. Getherm. Res. 67 (1995) 263–290.
[22] A. Neri, P. Papale, D. Del Seppia, R. Santacroce, Coupled conduit and atmospheric dispersal dynamics of the AD 79 Plinian eruption of Vesuvius, J. Volcanol. Geotherm. Res. 120 (2003) 141–160.
[23] G. Mastrolorenzo, Averno tuff ring in Campi Flegrei (south Italy), Bull. Volcanol. 54 (1994) 561–570.
[24] E. Stopler, Water in silicate glasses: an infrared spectroscopy study, Contrib. Mineral. Petrol. 81 (1982) 1–17.
[25] M.R. Carroll, J. Blank, Solubility of water in phonolitic melts, Am. Mineral. 82 (1997) 1111–1115.
[26] M.S. Ghiorso, R.O. Sack, Chemical Mass Transfer in Magmatic Processes IV. A revised and internally consistent thermodynamic model for the interpolation and extrapolation of liquid–solid equilibria in magmatic systems at elevated temperatures and pressures, Contrib. Mineral. Petrol. 119 (1995) 197–212.
[27] B.F. Houghton, C.J.N. Wilson, A vesicularity index for pyroclastic deposits, Bull. Volcanol. 51 (1989) 451–462.
[28] M.D. Higgins, Measurements of crystal size distributions, Am. Mineral. 85 (2000) 1105–1116.
[29] M.D. Higgins, Closure in crystal size distributions (CSD), verification of CSD calculations and the significance of CSD fans, Am. Mineral. 87 (2002) 171–175.
[30] M.J. Le Bas, R.W. Le Maitre, A. Streckeisen, B. Zanettin, A chemical classification of volcanic rocks based on the total alkali–silica diagram, J. Petrol. 27 (1986) 745–750.
[31] J.E. Hammer, K.V. Cashman, R.P. Hoblit, S. Newman, Degassing and microlite crystallization during pre-climatic events of the 1991 eruption of Mt. Pinatubo, Philippines, Bull. Volcanol. 60 (1999) 355–380.
[32] C. Martel, J.-L. Bourdier, M. Pichavant, H. Traineau, Textures, water content and degassing of silicic andesites from recent plinian and dome-forming eruptions at Mount Pelee volcano (Martinique, Lesser Antilees arc), J. Volcanol. Geotherm. Res. 96 (2000) 191–206.
[33] S. Noguchi, A. Toramaru, T. Stimano, Crystallization of microlites and degassing during magma ascent: constraints on the fluid mechanical behavior of magma during the Tenjo Eruption on Kozu Island, Japan, Bull. Volcanol. 68 (2006) 432–449.
[34] M. de' Gennaro, A. Incoronato, G. Mastrolorenzo, M.R. Adabbo, G. Spina, Depositional mechanisms and alteration processes in different types of pyroclastic deposits in Campi Flegrei volcanic field (Southern Italy), J. Volcanol. Geotherm. Res. 82 (1999) 113–137.
[35] C. Klug, K.V. Cashman, Vesiculation of May 18, 1980 Mount St. Helens magma, Geology 22 (1994) 468–472.
[36] B.D. Marsh, Crystal size distribution (CSD) in rocks and kinetics and dynamics of crystallization. I. Theory, Contrib. Mineral. Petrol. 99 (1988) 277–291.
[37] M.M. Morrissey, Long-period seismicity at Redoubt Volcano, Alaska, 1989–1990 related to magma degassing, J. Volcanol. Geotherm. Res. 75 (1997) 321–335.
[38] C. Martel, B.C. Schmidt, Decompression experiments as an insight into ascent rates of silicic magmas, Contrib. Mineral. Petrol. 144 (2003) 397–415.
[39] N. Thomas, C. Jaupart, S. Vergniolle, On the vesicularity of pumice, J. Geophys. Res. 99 (1994) 15633–15644.
[40] R.S.J. Sparks, The dynamics of bubble formation and growth in magmas: a review and new analysis, J. Volcanol. Geotherm. Res. 3 (1978) 1–37.
[41] Y. Zhang, A criterion for the fragmentation of bubbly magma based on brittle failure theory, Nature 402 (1999) 648–650.
[42] J. Marti, C. Soriano, D.B. Dingwell, Tube pumices as strain markers of the ductile–brittle transition during magma fragmentation, Nature 402 (1999) 650–653.
[43] O. Melnik, Fragmenting magma, Nature 397 (1999) 394–395.
[44] M.D. Higgins, J. Roberge, Crystal size distribution (CSD) of plagioclase and amphibole from Soufriere Hills volcano, Montserrat: evidence for dynamic crystallisation/textural coarsening cycles, J. Petrol. 44 (2003) 1401–1411.
[45] K.V. Cashman, S.M. McConnell, Multiple levels of magma storage during the 1980 summer eruptions of Mount St. Helens, WA, Bull. Volcanol. 68 (2005) 57–75.